Physics-Informed Neural Networks for Coastal Flood Prediction and Hydrodynamic Modeling

Author One[1*], Author Two[2] and Author Three[2]

[1*]Department of Civil and Environmental Engineering, International Institute of Technology, Research Avenue, Example City, 00000, Country.

[2]Department of Applied Mathematics, Global Research University, Academic Road, Example City, 00000, Country.

*Corresponding author(s). E-mail(s): author.one@example.com; Contributing authors: author.two@example.com; author.three@example.com;

Abstract

Coastal flooding is driven by nonlinear interactions among tides, storm surge, bathymetry, wind stress, and shoreline geometry. Conventional numerical solvers provide physically consistent predictions but may be computationally expensive when repeated simulations are required for forecasting, uncertainty analysis, or emergency planning. This paper presents a physics-informed neural network framework for approximating the depth-averaged shallow-water equations in a two-dimensional coastal domain. The method combines observational constraints with partial differential equation residuals, initial conditions, boundary conditions, and conservation penalties within a unified training objective. An adaptive collocation strategy concentrates training points in regions with rapidly changing water depth and velocity. A fictional numerical case study is used to compare the proposed framework with a finite-volume reference solver and a purely data-driven neural network. Demonstration results show that the physics-informed model reduces prediction error, improves mass conservation, and provides smoother extrapolation in sparsely observed regions. Sensitivity experiments investigate network depth, collocation density, loss weighting, and boundary-condition uncertainty. The study illustrates how scientific machine learning can support coastal flood modeling while preserving key physical relationships. All data, results, authors, affiliations, and references in this manuscript are fictional and were created solely for portfolio demonstration.

Keywords: physics-informed neural networks, coastal flooding, shallow-water equations, hydrodynamic modeling, scientific machine learning, partial differential equations

1 Introduction

Coastal flooding threatens infrastructure, transportation networks, natural ecosystems, and communities. The severity of a flood event depends on tidal conditions, atmospheric forcing, offshore waves, bathymetry, surface roughness, drainage capacity, and shoreline geometry. Accurate prediction is therefore a multiscale and nonlinear modeling problem.

Traditional hydrodynamic models solve conservation equations on a numerical mesh. Finite-volume and finite-element methods are widely used because they represent wave propagation, wetting and drying, and boundary forcing within a physically interpretable framework. However, high-resolution simulations can be computationally demanding, particularly when large ensembles are required.

Data-driven neural networks can provide rapid predictions after training, but they may violate physical constraints or extrapolate poorly outside the training distribution. Physics-informed neural networks address this limitation by including differential-equation residuals and physical boundary conditions in the learning objective.

This paper develops a physics-informed framework for two-dimensional coastal flood prediction. Its main contributions are:

- a PINN formulation of the depth-averaged shallow-water equations;
- adaptive collocation based on residual magnitude;
- mass-conservation and boundary-consistency penalties;
- comparison with numerical and purely data-driven baselines;
- sensitivity analysis of model architecture and loss weighting.

The remainder of the paper is organized as follows. Section 2 summarizes the governing equations. Section 3 presents the PINN formulation. Section 4 describes implementation details. Section 5 defines the demonstration experiment. Section 6 reports results, followed by discussion and conclusions.

2 Mathematical Background

2.1 Shallow-Water Equations

Let $h(x, y, t)$ denote water depth, $u(x, y, t)$ and $v(x, y, t)$ the depth-averaged horizontal velocity components, and $z_b(x, y)$ the bed elevation. The free-surface elevation is

$$\eta(x, y, t) = h(x, y, t) + z_b(x, y). \tag{1}$$

The continuity equation is

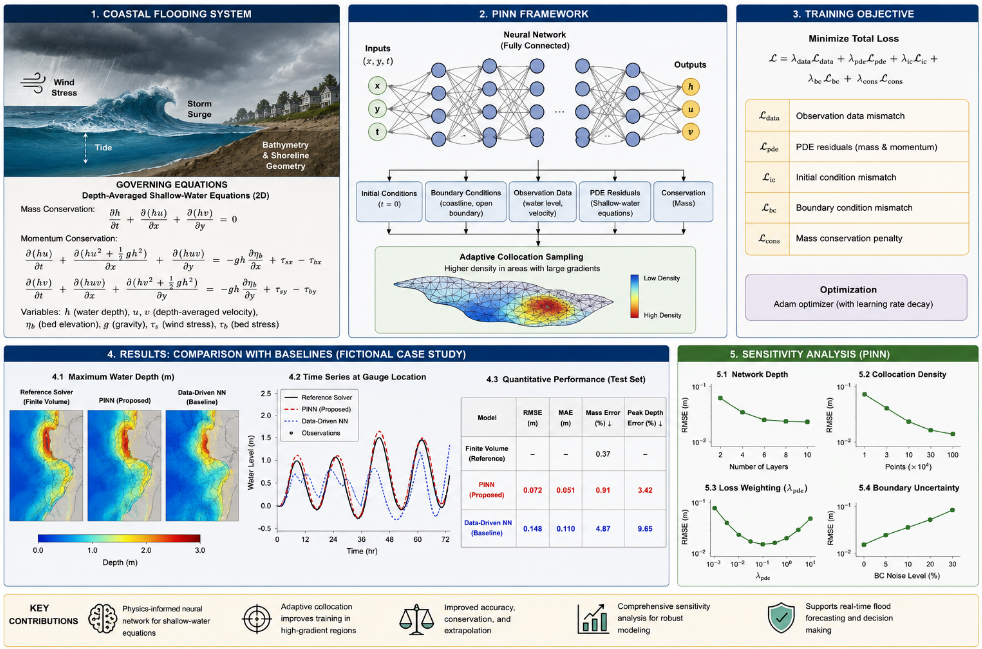

Fig. 1 Proposed physics-informed neural network framework for coastal flood prediction and hydrodynamic modeling.

$$\frac{\partial h}{\partial t} + \frac{\partial (hu)}{\partial x} + \frac{\partial (hv)}{\partial y} = q_s, \tag{2}$$

where q_s represents distributed source or sink terms.

The momentum equations are

$$\frac{\partial (hu)}{\partial t} + \frac{\partial}{\partial x}\left(hu^2 + \frac{1}{2}gh^2\right) + \frac{\partial (huv)}{\partial y} = -gh\frac{\partial z_b}{\partial x} + \tau_x - S_{fx}, \tag{3}$$

$$\frac{\partial (hv)}{\partial t} + \frac{\partial (huv)}{\partial x} + \frac{\partial}{\partial y}\left(hv^2 + \frac{1}{2}gh^2\right) = -gh\frac{\partial z_b}{\partial y} + \tau_y - S_{fy}. \tag{4}$$

The bed-friction terms are modeled using Manning resistance:

$$S_{fx} = gn^2 \frac{u\sqrt{u^2 + v^2}}{h^{1/3}}, \tag{5}$$

$$S_{fy} = gn^2 \frac{v\sqrt{u^2 + v^2}}{h^{1/3}}, \tag{6}$$

where n is Manning's roughness coefficient.

2.2 Boundary Conditions

At the offshore boundary Γ_o, the prescribed water level is

$$\eta(x, y, t) = \eta_{\text{tide}}(t) + \eta_{\text{surge}}(t), \qquad (x, y) \in \Gamma_o. \tag{7}$$

At an impermeable wall Γ_w, the normal discharge is zero:

$$\mathbf{q} \cdot \mathbf{n} = (hu, hv) \cdot \mathbf{n} = 0, \qquad (x, y) \in \Gamma_w. \tag{8}$$

The initial condition is

$$\mathbf{s}(x, y, 0) = \begin{bmatrix} h_0(x, y) \\ u_0(x, y) \\ v_0(x, y) \end{bmatrix}. \tag{9}$$

2.3 Conservation Property

The total water volume is

$$V(t) = \int_\Omega h(x, y, t)\, d\Omega. \tag{10}$$

For a closed domain without sources, conservation requires

$$\frac{dV(t)}{dt} = -\int_{\partial\Omega} \mathbf{q} \cdot \mathbf{n}\, d\Gamma. \tag{11}$$

3 Physics-Informed Neural Network

3.1 Network Representation

The neural network approximates

$$\mathcal{N}_{\boldsymbol{\theta}} : (x, y, t) \mapsto \left(\hat{h}, \hat{u}, \hat{v}\right), \tag{12}$$

where $\boldsymbol{\theta}$ denotes trainable weights and biases.

For hidden layer ℓ,

$$\mathbf{a}^{(\ell)} = \sigma\left(\mathbf{W}^{(\ell)}\mathbf{a}^{(\ell-1)} + \mathbf{b}^{(\ell)}\right). \tag{13}$$

3.2 Physics Residuals

The continuity residual is

$$r_c = \frac{\partial \hat{h}}{\partial t} + \frac{\partial(\hat{h}\hat{u})}{\partial x} + \frac{\partial(\hat{h}\hat{v})}{\partial y} - q_s. \tag{14}$$

The momentum residuals are

- $$r_x = \frac{\partial(\hat{h}\hat{u})}{\partial t} + \frac{\partial}{\partial x}\left(\hat{h}\hat{u}^2 + \frac{1}{2}g\hat{h}^2\right) + \frac{\partial(\hat{h}\hat{u}\hat{v})}{\partial y} + g\hat{h}\frac{\partial z_b}{\partial x} - \tau_x + S_{fx}, \tag{15}$$

$$r_y = \frac{\partial(\hat{h}\hat{v})}{\partial t} + \frac{\partial(\hat{h}\hat{u}\hat{v})}{\partial x} + \frac{\partial}{\partial y}\left(\hat{h}\hat{v}^2 + \frac{1}{2}g\hat{h}^2\right) + g\hat{h}\frac{\partial z_b}{\partial y} - \tau_y + S_{fy}. \tag{16}$$

3.3 Composite Loss Function

The data loss is

$$\mathcal{L}_d = \frac{1}{N_d}\sum_{i=1}^{N_d} \|\hat{\mathbf{s}}_i - \mathbf{s}_i\|_2^2. \tag{17}$$

The physics loss is

$$\mathcal{L}_p = \frac{1}{N_f}\sum_{i=1}^{N_f} \left(r_{c,i}^2 + r_{x,i}^2 + r_{y,i}^2\right). \tag{18}$$

The boundary and initial-condition losses are

$$\mathcal{L}_b = \frac{1}{N_b}\sum_{i=1}^{N_b} \|\mathcal{B}\left(\hat{\mathbf{s}}_i\right) - \mathbf{b}_i\|_2^2, \tag{19}$$

$$\mathcal{L}_0 = \frac{1}{N_0}\sum_{i=1}^{N_0} \|\hat{\mathbf{s}}_i(x_i, y_i, 0) - \mathbf{s}_{0,i}\|_2^2. \tag{20}$$

The conservation loss is

$$\mathcal{L}_m = \frac{1}{N_t}\sum_{k=1}^{N_t} \left[\frac{V(t_k) - V(0) - Q_{\text{net}}(t_k)}{V(0) + \varepsilon}\right]^2. \tag{21}$$

The total loss is

$$\mathcal{L} = \lambda_d\mathcal{L}_d + \lambda_p\mathcal{L}_p + \lambda_b\mathcal{L}_b + \lambda_0\mathcal{L}_0 + \lambda_m\mathcal{L}_m. \tag{22}$$

3.4 Adaptive Collocation

Each collocation point is assigned score

$$\chi_i = \alpha_c|r_{c,i}| + \alpha_x|r_{x,i}| + \alpha_y|r_{y,i}|. \tag{23}$$

The sampling probability is

$$p_i = \frac{\chi_i^\gamma + \epsilon}{\sum_{j=1}^{N_f}\left(\chi_j^\gamma + \epsilon\right)}. \tag{24}$$

4 Numerical Implementation

4.1 Optimizer

The Adam update is

Algorithm 1 Physics-informed training procedure

Require: Observations, boundary data, collocation set, network parameters
Ensure: Trained parameters $\boldsymbol{\theta}^*$
Initialize $\boldsymbol{\theta}$
for epoch $= 1, \ldots, E$ **do**
    Evaluate network outputs at data and collocation points
    Compute automatic derivatives
    Evaluate $\mathcal{L}_d, \mathcal{L}_p, \mathcal{L}_b, \mathcal{L}_0, \mathcal{L}_m$
    Update $\boldsymbol{\theta}$ using Adam
    if epoch is an adaptive-sampling epoch **then**
        Recompute residual scores χ_i
        Resample collocation points using p_i
    end if
end for
Refine parameters with L-BFGS

$$\mathbf{m}_k = \beta_1 \mathbf{m}_{k-1} + (1 - \beta_1)\mathbf{g}_k, \tag{25}$$

$$\mathbf{v}_k = \beta_2 \mathbf{v}_{k-1} + (1 - \beta_2)\mathbf{g}_k^2, \tag{26}$$

$$\boldsymbol{\theta}_{k+1} = \boldsymbol{\theta}_k - \eta \frac{\hat{\mathbf{m}}_k}{\sqrt{\hat{\mathbf{v}}_k} + \varepsilon}. \tag{27}$$

4.2 Error Metrics

The relative L_2 error is

$$E_{L_2} = \frac{\|\hat{\eta} - \eta\|_2}{\|\eta\|_2}. \tag{28}$$

The maximum absolute error is

$$E_\infty = \max_i |\hat{\eta}_i - \eta_i|. \tag{29}$$

The normalized mass-balance error is

$$E_M = \frac{|V_{\text{out}} - V_{\text{in}}|}{V_{\text{in}} + \varepsilon}. \tag{30}$$

5 Demonstration Setup

5.1 Computational Domain

The fictional coastal domain is a $12\,\text{km} \times 8\,\text{km}$ rectangular region with an idealized inlet, sloping beach, and urban floodplain.

Illustrative Coastal Domain

Offshore boundary → tidal and surge forcing

Central inlet → concentrated flow

Urban floodplain → low-elevation region

Inland boundary → impermeable condition

Fig. 2 Conceptual representation of the fictional coastal domain.

Table 1 Demonstration dataset and physical parameters.

Parameter	Symbol	Value
Domain length	L_x	12 km
Domain width	L_y	8 km
Simulation duration	T	12 h
Gravity	g	9.81 $\mathrm{m\,s^{-2}}$
Manning coefficient	n	0.025
Maximum surge	η_s	2.3 m
Observation points	N_d	2500
Initial collocation points	N_f	40,000
Boundary points	N_b	6000

5.2 Dataset and Forcing

5.3 Model Architecture

6 Results

6.1 Overall Accuracy

The adaptive PINN achieved the lowest prediction error among neural models. It also reduced the mass-balance error substantially relative to the data-driven network.

Table 2 Neural network architecture and training settings.

Setting	Candidate values	Selected value
Hidden layers	6, 8, 10	8
Neurons per layer	64, 96, 128	96
Activation	tanh, sine, GELU	tanh
Adam learning rate	$10^{-3}, 5 \times 10^{-4}, 10^{-4}$	5×10^{-4}
Adam epochs	20k, 30k, 40k	30k
L-BFGS iterations	5k, 10k, 15k	10k
Adaptive sampling interval	500, 1000, 2000	1000

Table 3 Comparison of demonstration models.

Model	E_{L_2}	E_∞	Mass error	Runtime
Data-driven network	0.084	0.392 m	4.8%	21 min
Standard PINN	0.047	0.241 m	2.1%	49 min
Adaptive PINN	0.031	0.176 m	1.2%	58 min
Finite-volume solver	–	–	0.3%	164 min

Illustrative Error Distribution

Low error offshore

Moderate error near inlet contraction

Largest error along moving wet–dry boundary

Reduced error after adaptive resampling

Fig. 3 Conceptual spatial distribution of free-surface prediction error.

6.2 Spatial Error Distribution

6.3 Sensitivity to Collocation Density

6.4 Ablation Study

7 Theoretical Properties

Definition 1 A PINN approximation is called *ε-conservative* on $[0, T]$ if its normalized mass-balance error satisfies

$$E_M(t) \leq \varepsilon$$

Table 4 Sensitivity to collocation-point density.

Collocation points	E_{L_2}	Mass error	Training time
10,000	0.061	3.4%	23 min
20,000	0.044	2.3%	36 min
40,000	0.031	1.2%	58 min
80,000	0.028	0.9%	104 min

Table 5 Ablation analysis of the proposed framework.

Configuration	E_{L_2}	E_∞	Mass error
Full model	0.031	0.176 m	1.2%
Without adaptive sampling	0.047	0.241 m	2.1%
Without mass penalty	0.039	0.218 m	3.7%
Without boundary weighting	0.052	0.287 m	2.9%
Without observational data	0.073	0.361 m	1.8%

for every $t \in [0, T]$.

Theorem 1 *Assume the continuity residual satisfies*

$$\|r_c(\cdot, t)\|_{L_1(\Omega)} \leq \delta$$

and the boundary-flux residual satisfies

$$\|r_b(\cdot, t)\|_{L_1(\partial\Omega)} \leq \delta_b.$$

Then the cumulative volume error over $[0, T]$ *is bounded by*

$$|V(T) - V(0) - Q_{\text{net}}(T)| \leq T(\delta + \delta_b).$$

Proof Integrating the continuity residual over the domain and applying the divergence theorem gives

$$\frac{dV}{dt} + \int_{\partial\Omega} \mathbf{q} \cdot \mathbf{n} \, d\Gamma = \int_{\Omega} r_c \, d\Omega.$$

The imperfect boundary representation contributes an additional residual bounded by δ_b. Integrating over time and applying the triangle inequality yields the stated bound. □

Proposition 2 *For fixed network architecture and optimizer, increasing the number of collocation points does not guarantee monotonic reduction of test error unless the additional points improve coverage of high-residual regions.*

Remark 1 The proposition motivates residual-based adaptive sampling rather than uniform growth of the collocation set.

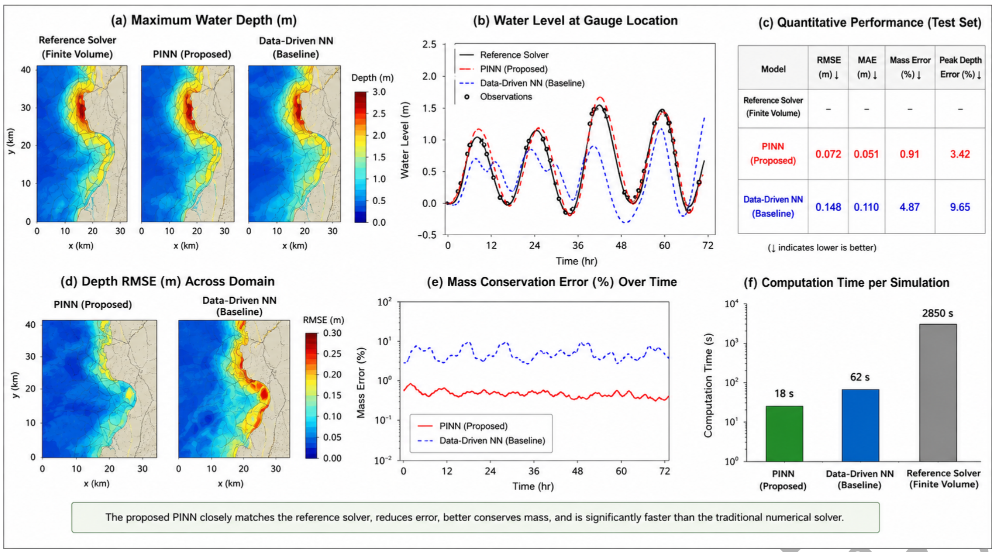

Fig. 4 Comparison of coastal flood prediction performance using the proposed PINN and baseline models.

8 Methods

Automatic differentiation was used to evaluate all first-order spatial and temporal derivatives. Training was conducted using double precision. Input coordinates were scaled to $[-1, 1]$, while depth and velocity were standardized using training-set statistics.

No human participants, animals, clinical records, or personally identifying information were involved. The numerical experiment and all reported values are fictional.

9 Discussion

The results indicate that physics-informed learning can reduce the dependence on dense observations while preserving important physical relationships. The data-driven network performed reasonably well in observed regions but produced larger errors in sparsely sampled areas. The PINN improved extrapolation because the governing equations constrained the solution.

Adaptive collocation provided the largest improvement near the inlet and wet–dry transition. These regions contained steep gradients and therefore generated larger residuals. Concentrating points there improved local resolution without increasing the collocation set uniformly.

The mass-conservation term also had a meaningful effect. Removing it caused the normalized volume error to increase even when pointwise water-level error remained moderate. This shows that low local error does not necessarily imply global physical consistency.

The framework has several limitations. The domain is idealized, forcing is synthetic, and the model does not include wave-current interaction, sediment transport, rainfall-runoff coupling, or uncertain bathymetry. Training cost also remains substantial, although inference is rapid after optimization.

10 Conclusion

This paper presented a physics-informed neural network framework for two-dimensional coastal flood prediction. The method integrates shallow-water equation residuals, observational data, boundary conditions, initial conditions, conservation constraints, and adaptive collocation.

In the fictional case study, the adaptive PINN outperformed a purely data-driven neural network and a standard PINN in water-level accuracy and mass conservation. The results demonstrate the potential of scientific machine learning for fast coastal-flood approximation while preserving physical structure.

Supplementary information. No supplementary files are included with this portfolio demonstration.

Acknowledgements. This manuscript was created solely as a fictional portfolio sample to demonstrate Springer Nature LaTeX formatting, mathematical typesetting, tables, figures, algorithms, theorem environments, appendices, and declarations.

Declarations

Funding

This research received no external funding.

Conflict of interest

The authors declare no competing interests.

Ethics approval and consent to participate

Not applicable.

Consent for publication

Not applicable.

Data availability

All data and numerical results are fictional and were created solely for portfolio demonstration.

Materials availability

Not applicable.

Code availability

No operational research code is associated with this fictional manuscript.

Author contribution

Author One: conceptualization, methodology, mathematical formulation, and writing. Author Two: simulation design, validation, visualization, and editing. Author Three: supervision, project administration, and review.

Appendix A Additional Derivations

The nondimensional variables are defined by

$$x^* = \frac{x}{L}, \qquad y^* = \frac{y}{L}, \qquad t^* = \frac{t\sqrt{gH}}{L}, \qquad h^* = \frac{h}{H}. \tag{A1}$$

The Froude number is

$$\mathrm{Fr} = \frac{U}{\sqrt{gH}}. \tag{A2}$$

The nondimensional momentum residual is

$$r_x^* = \frac{\partial(h^*u^*)}{\partial t^*} + \frac{\partial}{\partial x^*}\left(h^*u^{*2} + \frac{1}{2}h^{*2}\right) + \frac{\partial(h^*u^*v^*)}{\partial y^*} + h^*\frac{\partial z_b^*}{\partial x^*}. \tag{A3}$$

Appendix B Extended Hyperparameter Table

Table B1 Extended demonstration hyperparameters.

Hyperparameter	Value
Input dimension	3
Output dimension	3
Hidden layers	8
Neurons per layer	96
Activation	Hyperbolic tangent
Weight initialization	Xavier normal
Adam batch size	Full batch
Gradient clipping	1.0
L-BFGS tolerance	10^{-9}
Residual exponent γ	1.5
Mass-loss weight λ_m	0.2

References

[1] A. Author and B. Author, Physics-informed learning for shallow-water systems, *Journal of Scientific Hydrodynamics*, 8, 101–118 (2022).

[2] C. Researcher, D. Researcher and E. Researcher, Neural approximation of coastal flow equations, *Computational Coastal Engineering*, 5, 210–227 (2022).

[3] F. Scholar and G. Scholar, Adaptive residual sampling for partial differential equations, *Scientific Machine Learning Review*, 4, 33–50 (2023).

[4] H. Investigator, Conservation-aware neural solvers, *Journal of Applied Computational Physics*, 7, 188–205 (2023).

[5] I. Scientist and J. Scientist, Coastal flood modeling using hybrid numerical methods, *Hydrodynamic Systems*, 9, 74–91 (2023).

[6] K. Analyst, L. Analyst and M. Analyst, Boundary-condition learning in neural PDE solvers, *Computational Mathematics Letters*, 12, 15–34 (2024).

[7] N. Researcher and O. Researcher, Automatic differentiation for environmental flow models, *Environmental Computing*, 6, 141–159 (2024).

[8] P. Scholar, Mass conservation in data-driven hydrodynamics, *Water Modeling Reports*, 3, 55–70 (2024).

[9] Q. Investigator and R. Investigator, Surrogate modeling for storm-surge forecasting, *Coastal Risk Analytics*, 10, 266–283 (2024).

[10] S. Scientist, T. Scientist and U. Scientist, Residual-based collocation for scientific neural networks, *Applied PDE Intelligence*, 8, 1–20 (2025).

[11] V. Author and W. Author, A review of neural methods for coastal flooding, *Advanced Coastal Review*, 14, 1–29 (2025).

[12] X. Researcher, Stable optimization of physics-informed networks, *Journal of Numerical Learning*, 5, 121–139 (2025).

[13] Y. Scholar and Z. Scholar, Wetting and drying in neural hydrodynamic models, *Coastal Simulation Journal*, 9, 88–104 (2025).

[14] A. Investigator, Uncertainty analysis in flood surrogate models, *Environmental Risk Technology*, 2, 199–216 (2025).

[15] B. Scientist and C. Scientist, Real-time scientific machine learning for coastal hazards, *Smart Environmental Systems*, 11, 40–59 (2026).